JACS
JOURNAL OF THE AMERICAN CHEMICAL SOCIETY

pubs.acs.org/JACS
Article

Location of Phosphorylation Sites within Long Polypeptide Chains by Binder-Assisted Nanopore Detection

Wei-Hsuan Lan, Hanxiao He, Hagan Bayley,* and Yujia Qing*

Cite This: J. Am. Chem. Soc. 2024, 146, 24265−24270

Read Online

ACCESS | Metrics & More | Article Recommendations | Supporting Information

ABSTRACT: The detection and mapping of protein phosphorylation sites are essential for understanding the mechanisms of various cellular processes and for identifying targets for drug development. The study of biopolymers at the single-molecule level has been revolutionized by nanopore technology. In this study, we detect protein phosphorylation within long polypeptides (>700 amino acids), after the attachment of binders that interact with phosphate monoesters; electro-osmosis is used to drive the tagged chains through engineered protein nanopores. By monitoring the ionic current carried by a nanopore, phosphorylation sites are located within individual polypeptide chains, providing a valuable step toward nanopore proteomics.

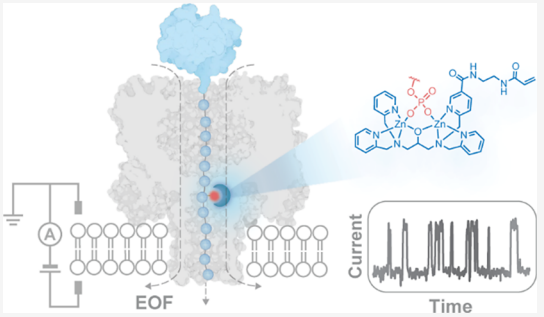

INTRODUCTION

Post-translational modifications (PTMs) of proteins are pivotal in cell regulation and typically involve the enzymatic addition of chemical groups to amino acid side chains.[1] Phosphorylation, the process of adding a phosphate group to predominantly serine, threonine, and tyrosine residues, is the most prevalent PTM, with over ∼10^6 phosphorylation sites that account for >60% of all reported PTMs.[1] Dysregulation of phosphorylation is commonly associated with diseases such as cancer, Parkinson's, and Alzheimer's.[2] For example, tau proteins in pathological lesions of Alzheimer's are heterogeneously and highly phosphorylated, with more than 50 identified phosphorylation sites.[3] Bottom-up mass spectrometry is routinely applied to detect PTMs on peptide fragments derived from disease-related proteins but faces challenges to determine if widely separated modifications, whether identical or distinct, are present on the same polypeptide chain. For example, cross-talk between phosphorylation and *O*-GlcNAcylation was reported to regulate subcellular localization of proteins, such as tau.[4] However, there lacks a straightforward technique to correlate the presence of PTMs at distant sites within individual polypeptide chains.[5] Nanopore nucleic acid sequencing has emerged as a powerful technology to provide ultralong DNA or RNA reads for long-range correlation of genomic or transcriptomic features.[6,7] Single-molecule sensing using protein nanopores therefore holds great potential for single-molecule analysis of full-length proteoforms.[8−12] Electro-osmosis has been demonstrated to propel unfolded polypeptides through nanopores[13−15] and PTMs deep within long polypeptide chains have been located during translocation.[14] This work is a first step toward the label-free analysis of modified proteins extracted from biological samples.[14] In parallel, the identification of PTMs on short peptides (up to ∼30 amino acids) has been achieved,[16−19] either when the peptides are sensed as a whole or when a peptide is transported through the pore as a conjugate to an oligonucleotide.[18] Although PTMs containing branched structures (e.g., glycans) or entire proteins (e.g., ubiquitin) might be challenging to detect on polypeptides translocating through nanopores of ∼1−2 nm in internal diameter, >80% of the ∼400 PTM types are small (<∼300 Da) or narrow in shape.[1] In addition, nanopores with wider internal geometries (e.g., ClyA) might be applicable for sensing bulkier PTMs. To demonstrate the broad applicability of the approach, we previously detected three PTMs (phosphorylation, glutathionylation, and glycosylation) on full-length proteins when segments of singly modified individual thioredoxin (Trx)-linker concatemers were stalled during translocation through a nanopore.[14] To our surprise, glutathionylation and phosphorylation, placed at a particular site in the polypeptide, produced similar current blockades and noise patterns.[14] This prompts the question of how many PTMs can be discriminated among the 400 different natural PTMs identified so far by their perturbation to the ionic current driven through a protein nanopore.[1] To distinguish PTMs with similar electrical signatures or to allow targeted detection of specific PTMs, we sought to use PTM-specific binders to generate distinct current characteristics. To this end, we have explored a phosphorylation-specific reversible chemical binder, Phos-tag,

Received: March 19, 2024
Revised: June 21, 2024
Accepted: June 24, 2024
Published: July 10, 2024

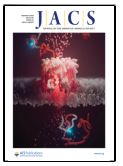

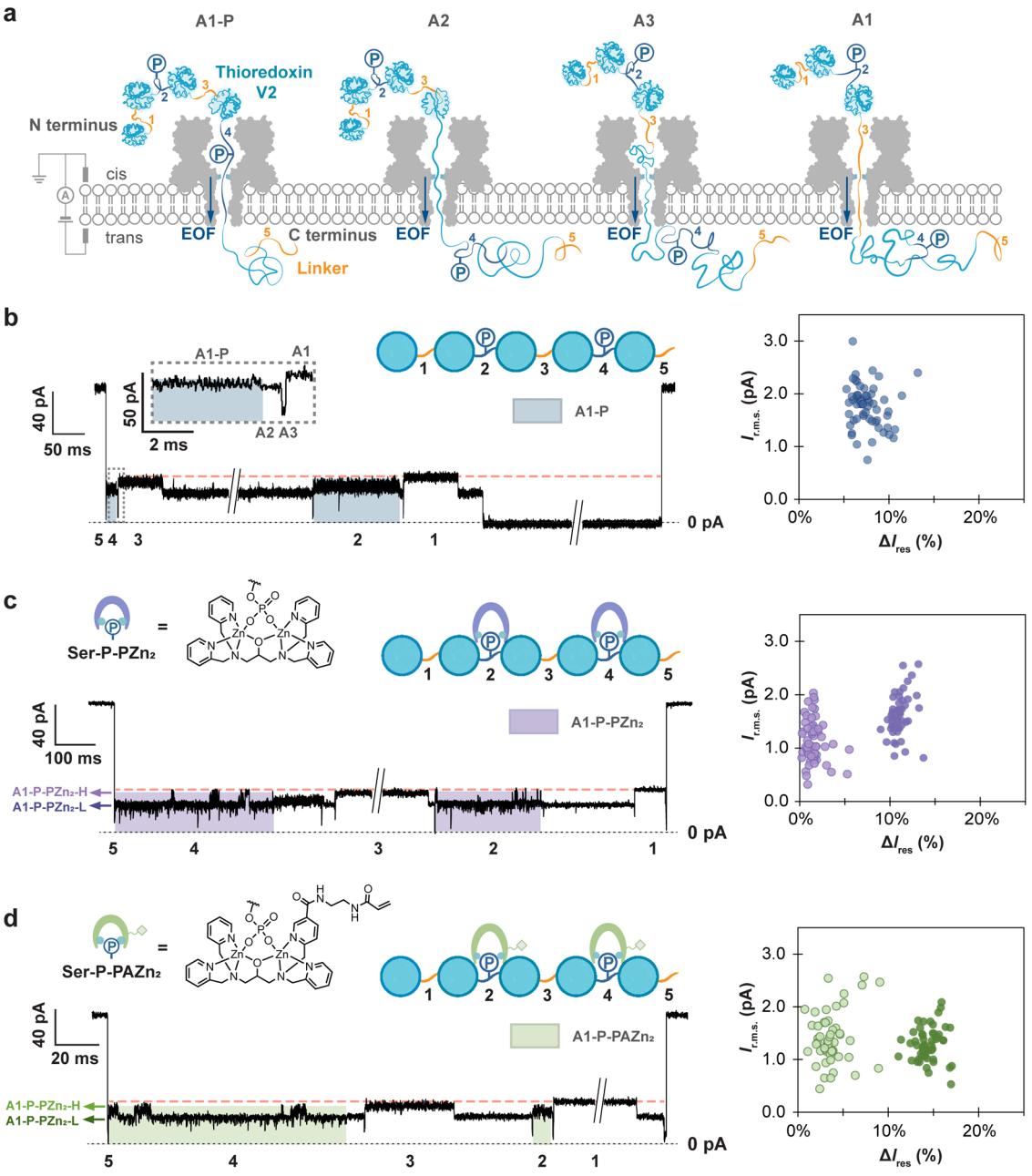

Figure 1. Detection of serine phosphate bound to Phos-tag in a polypeptide chain. (a) Monitoring the Trx-linker pentamer traversing the α-hemolysin nanopore $(NN\text{-}113R)_7$. The Trx-linker pentamer contained two RRAS sequences within linker 2 and linker 4, which were phosphorylated enzymatically on serine. (b) Left: phosphorylated serine residues (Ser-P) 274 amino acids apart on a Trx-linker pentamer were detected. Level A1 for linker 3 showed a slightly lower $I_{res\%}$ compared to that of linker 1 ($I_{res\%}$ of linker 1 is shown in orange dash). This difference was attributed to the additional amino acid sequence in linker 3 (Table S1). Right: scatter plot of $I_{r.m.s.}$ and $\Delta I_{res\%}$ for individual translocation events, $\Delta I_{res\%} = I_{res\%}(\text{A1, linker 1}) - I_{res\%}(\text{A1-P})$, where $I_{res\%}(\text{A1, linker 1})$ is the $I_{res\%}$ value of the A1 level for linker 1 within an individual translocation event. If there were two Ser-P molecules detected in different segments within a single translocation event, they were analyzed individually. (c) Left: Phos-tag dizinc complexes bound to phosphoserine generated alternating current levels (A1-P-PZn_2). Right: scatter plot of $I_{r.m.s.}$ and $\Delta I_{res\%}$ for individual translocation events. Data points in light purple are the $I_{r.m.s.}$ and $\Delta I_{res\%}$ values for the higher level of the two-level A1 state (A1-P-PZn_2-H), while data points in dark purple are the $I_{r.m.s.}$ and $\Delta I_{res\%}$ values for the lower level of the two-level A1 state (A1-P-PZn_2-L). (d) Left: Phos-tag-acrylamide dizinc complexes bound to serine phosphate produced alternating current levels (A1-P-$PAZn_2$). Right: scatter plot of $I_{r.m.s.}$ and $\Delta I_{res\%}$ for individual translocation events. Data points in light green are the $I_{r.m.s.}$ and $\Delta I_{res\%}$ values for the higher level of the two-level A1 state (A1-P-$PAZn_2$-H), while data points in dark green are the $I_{r.m.s.}$ and $\Delta I_{res\%}$ values for the lower level of the two-level A1 state (A1-P-$PAZn_2$-L). If there were two A1-P-PZn_2 or A1-P-$PAZn_2$ detected in different segments in a single translocation event, they were analyzed individually. Conditions in (b): 10 mM HEPES, pH 7.2, 750 mM GdnHCl, and 2.37 μM Trx-linker pentamer (*cis*). Conditions in (c): 10 mM HEPES, pH 7.2, 750 mM GdnHCl, 2.37 μM Trx-linker pentamer (*cis*), 118.5 μM Phos-tag (*cis*), and 237 μM $ZnCl_2$ (*cis*). Condition in (d): 10 mM HEPES, pH 7.2, 750 mM GdnHCl, 2.37 μM Trx-linker pentamer (*cis*), 118.5 μM Phos-tag-acrylamide (*cis*), and 237 μM $ZnCl_2$ (*cis*). All of the measurements were conducted at +140 mV (*trans*) and 23 ± 1 °C.

https://doi.org/10.1021/jacs.4c03912
J. Am. Chem. Soc. 2024, 146, 24265−24270

which binds selectively and strongly to phosphate monoesters when complexed with zinc ions (e.g., for phosphoserine or phosphothreonine residues within model peptides, K_d = ~0.7 μM; for phosphotyrosine residues within model peptides, K_d = ~70 nM; for SO_4^{2-}, K_d = ~130 μM; for Cl^-, K_d = ~2 mM).[20,21] Phos-tag produced distinctive modulation of the associated ionic current as phosphorylated polypeptide chains were translocated through an engineered nanopore, thereby mediating enhanced localization of phosphorylation sites within long polypeptide chains.

RESULTS AND DISCUSSION

In our previous research, we employed an anion-selective α-hemolysin (αHL) mutant $(NN\text{-}113R)_7$ (permeability ratio P_{Na^+}/P_{Cl^-} = 0.33)[22] to generate electro-osmotic flow, thereby driving the capture, linearization, and translocation of polypeptide chains. We identified and located PTMs on long polypeptide chains of up to nine thioredoxin units (Trx, 108 amino acids (aa)) connected by linkers (29 aa).[14] Each Trx unit within the Trx-linker concatemers had the two catalytic cysteines removed (Trx: C32S/C35S).[8] Chaotropic reagents (e.g., guanidinium chloride (GdnHCl) or urea) at non-denaturing concentrations were used to promote cotranslocational unfolding.[14] During the electro-osmotic translocation of the Trx-linker concatemers, features comprising three levels were seen (A1, A2, and A3) (Figure 1a,b). We provisionally assigned level A1 to be produced by the nanopore containing a threaded linker ahead of a folded Trx unit, level A2 to be produced when a partially unfolded C-terminus of a Trx unit extends into the nanopore, and level A3 to be produced by the spontaneous unfolding and passage of the remaining Trx polypeptide chain through the nanopore. In the presence of a PTM in the linker, a phosphate group (P), for instance, level A1 exhibited a reduced percentage residual current ($I_{res\%}$) value and higher root-mean-square noise ($I_{r.m.s.}$)[14] (Figure 1b).

Here, we examined the detection of phosphorylation in association with phosphate-specific binders: Phos-tag dizinc complex (PZn_2) and Phos-tag-acrylamide dizinc complex ($PAZn_2$). Phos-tag is commonly immobilized in SDS-PAGE gels to detect phosphoproteins[23,24] and applied to generate mass shifts in MALDI-TOF mass spectrometry.[25] We constructed a Trx-linker pentamer ($(Trx\text{-}linker)_5$) containing two phosphorylation sites (RRAS) in linker 2 and linker 4 (Figures 1a, S1, and Table S1), which were phosphorylated on serine by the catalytic subunit of protein kinase A (Figure S2). Phosphorylated polypeptides were captured, unfolded, and translocated by electro-osmosis through the $(NN\text{-}113R)_7$ αHL pore. GdnHCl (750 mM) was employed to accelerate cotranslocational unfolding. Consistent with prior findings, translocation of the pentamer, C-terminus first, generated current patterns with a maximum of 4 A1−A3 repeats following an initial spike (Figure 1b). The spike to around 0 pA at the beginning of nearly all the translocation events was attributed to rapid unfolding and translocation of the first C-terminal Trx-linker unit. While only ~6% of the doubly phosphorylated Trx-linker pentamers produced 4 repeating A1−A3 features following an initial spike, >72% of the recorded translocation events contained at least one A1 level with a reduced $I_{res\%}$ value and a higher $I_{r.m.s.}$, compared to A1 levels for unmodified segments (Table S2). These characteristics were consistent with the electrical profiles previously identified for a phosphorylated linker and were therefore assigned as level A1-P. In events where 4 repeats of A1−A3 features were observed following an initial spike, the level A1-P was recorded for both the second and fourth units, consistent with the presence of two phosphorylated serine residues (Ser-P) within linker 2 and linker 4, 274 amino acids apart within the polypeptide chain.

To determine whether the binding of PZn_2 and $PAZn_2$ to phosphates in the polypeptide chains could be identified during translocation, we preformed complexes of phosphorylated Trx-linker pentamer with PZn_2 and $PAZn_2$, individually, with a molar ratio of $(Trx\text{-}linker)_5$:Phos-tag or Phos-tag-acrylamide:$ZnCl_2$ = 1:50:100 (10 mM HEPES, pH 7.2, 750 mM GdnHCl, 58.4 μM Trx-linker pentamer, 2.92 mMPhos-tag or Phos-tag-acrylamide, 5.84 mM $ZnCl_2$), and added the mixture to the cis compartment of the recording chamber (composition of recording solution: 10 mM HEPES, pH 7.2, 750 mM GdnHCl, 2.37 μM Trx-linker pentamer, 118.5 μM Phos-tag or Phos-tag-acrylamide, 237 μM $ZnCl_2$). While the unmodified segments exhibited A1 levels characteristic of the unphosphorylated linkers, the phosphorylated linkers generated a distinctive A1 state with an ionic current that alternated between two levels (Figure 1c,d). The percentage residual currents of the two levels resulted from PZn_2 binding were both smaller compared to those from $PAZn_2$ ($\Delta I_{res\%}$ for the higher level of the alternating current steps = 1.6 ± 1.0% for PZn_2 and 3.8 ± 1.7% for $PAZn_2$; $\Delta I_{res\%}$ for the lower level of the alternating steps = 11 ± 1% for PZn_2 and 14 ± 1% for $PAZn_2$) (Figure 1c,d and Table S2). We attributed the larger current blockade to the acrylamide appendage in $PAZn_2$ and continued to investigate binder-assisted PTM detection using $PAZn_2$. To verify whether the distinctive current feature stemmed from the association of $PAZn_2$ and Ser-P in the Trx-linker pentamer, a competition assay was performed in which excess phosphoserine was introduced to compete for binding with $PAZn_2$ (Methods and Figure S3). Nanopore characterization of the phosphorylated Trx-linker pentamers complexed with $PAZn_2$ (preformed at a molar ratio of $(Trx\text{-}linker)_5$:Phos-tag-acrylamide:$ZnCl_2$ = 1:50:100 (10 mM HEPES, pH 7.2, 750 mM GdnHCl, 58.4 μM Trx-linker pentamer, 2.92 mM Phos-tag-acrylamide, 5.84 mM $ZnCl_2$)) was first recorded for approximately 10 min (composition of recording solution in cis compartment: 10 mM HEPES, pH 7.2, 750 mM GdnHCl, 2.37 μM Trx-linker pentamer, 118.5 μM Phos-tag or Phos-tag-acrylamide, 237 μM $ZnCl_2$) (Methods). Subsequently, excess phosphoserine was added to the cis compartment (237 μM), and another 10 min recording was performed. Prior to the addition of phosphoserine, 81% of the A1-P levels (N = 29) exhibited two alternating steps. The frequency of these events dropped to 17% (N = 24) after the addition of phosphoserine. The alternating levels were not observed in the presence of excess $ZnCl_2$ without Phos-tag-acrylamide (10 mM HEPES, pH 7.2, 750 mM GdnHCl, 2.37 μM Trx-linker pentamer, 2 mM $ZnCl_2$) (Figure S4). These results suggest that state A1 with two interconverting levels arose from the binding of $PAZn_2$ to Ser-P (henceforth A1-P-$PAZn_2$). Transitions between the A1-P-$PAZn_2$ level and a level with an ionic current closely similar to level A1-P were also detected (Figure S5), which were attributed to the dissociation of $PAZn_2$ from Ser-P while the phosphorylated polypeptide segment was within the pore. The two current levels in A1-P-$PAZn_2$ likely reflect the two-step chelation of a phosphate monoester with $PAZn_2$.[26−28] A kinetic analysis revealed that the level with larger current blockades (A1-P-$PAZn_2$-L) had a mean dwell time that was ~6 times longer than the level with smaller

https://doi.org/10.1021/jacs.4c03912
J. Am. Chem. Soc. 2024, 146, 24265−24270

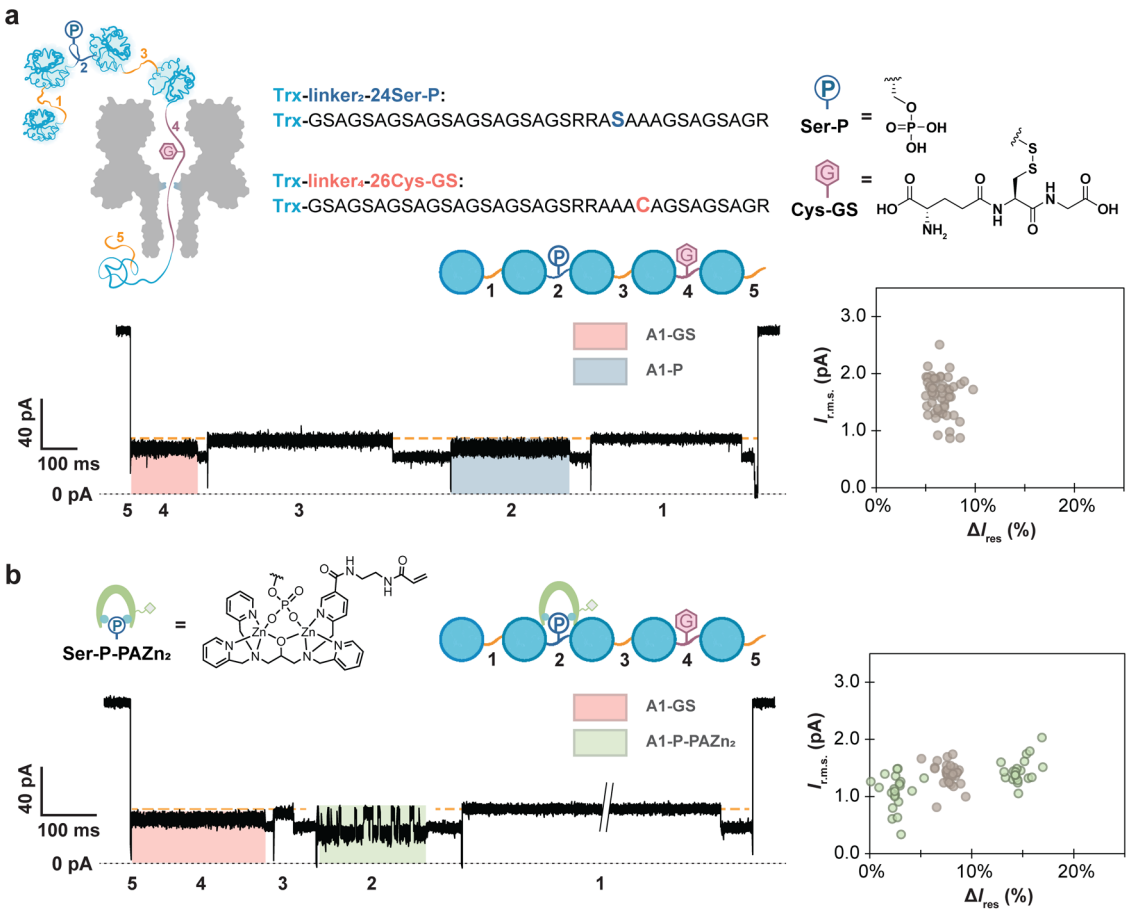

Figure 2. Detection of phosphorylation and glutathionylation in a Trx-linker pentamer in the presence of Phos-tag. (a) The blockades and noise from Ser-P and Cys-GS cannot be readily discriminated. Top and bottom-left: monitoring of the phosphorylated and glutathionylated Trx-linker pentamer during translocation through a $(NN\text{-}113R)_7$ αHL nanopore. The pentamer is phosphorylated on Ser-24 (Ser-P) of linker 2 and glutathionylated on the Cys-26 (Cys-GS) of linker 4. Bottom-right: scatter plot of $I_{r.m.s.}$ and $\Delta I_{res\%}$ for individual translocation events, $\Delta I_{res\%} = I_{res\%}(A1, \text{linker } 1) - I_{res\%}(A1^*)$, where $I_{res\%}(A1, \text{linker } 1)$ is the $I_{res\%}$ value of the A1 level for linker 1 within an individual translocation event and $I_{res\%}(A1^*)$ is the $I_{res\%}$ value of A1-GS or A1-P. If there were two A1* detected in different segments within a single translocation event, they were analyzed individually. (b) $PAZn_2$ produced an additional current feature when bound to Ser-P. Left: monitoring the phosphorylated and glutathionylated Trx-linker pentamer in the presence of $PAZn_2$ during translocation through a $(NN\text{-}113R)_7$ αHL nanopore. Right: scatter plot of $I_{r.m.s.}$ and $\Delta I_{res\%}$ for individual translocation events. Data points in gray are the $I_{r.m.s.}$ and $\Delta I_{res\%}$ values for A1-GS and A1-P, while data points in green are the $I_{r.m.s.}$ and $\Delta I_{res\%}$ values for the higher and lower levels of the two-level A1 state (A1-P-$PAZn_2$-H and A1-P-$PAZn_2$-L). Conditions in (a): 10 mM HEPES, pH 7.2, 750 mM GdnHCl, 2.37 μM Trx-linker pentamer (*cis*), +140 mV (*trans*), 23 ± 1 °C. Conditions in (b): 10 mM HEPES, pH 7.2, 750 mM GdnHCl, 2.37 μM Trx-linker pentamer (*cis*), 118.5 μM Phos-tag-acrylamide (*cis*), 237 μM $ZnCl_2$ (*cis*), +140 mV (*trans*), 23 ± 1 °C.

current blockades (A1-P-$PAZn_2$-H) ($\langle\tau_{A1\text{-}P\text{-}PAZn2\text{-}L}\rangle$ = 15.1 ± 0.1 ms, $\langle\tau_{A1\text{-}P\text{-}PAZn2\text{-}H}\rangle$ = 2.7 ± 0.1 ms), indicating that level A1-P-$PAZn_2$-L was the more stable binding state (Table S3). We suggest that level A1-P-$PAZn_2$-L represents $PAZn_2$ with both zinc ions chelated by phosphate oxygen atoms, and level A1-P-$PAZn_2$-H, $PAZn_2$ with only one zinc ion chelated by a phosphate oxygen atom.

To ensure complete detection of phosphorylated sites within the Trx-linker pentamer, we further optimized the recording conditions using $PAZn_2$. Increasing the binder concentration to 1000 equiv over Trx-linker pentamer resulted in almost complete detection of $PAZn_2$-bound Ser-P (83% at 10 mM HEPES, pH 7.2, 750 mM GdnHCl, 2.37 μM Trx-linker pentamer, 118.5 μM Phos-tag-acrylamide, 237 μM $ZnCl_2$ ($(Trx\text{-}linker)_5$:Phos-tag-acrylamide:$ZnCl_2$ = 1:50:100) versus 95% at 10 mM HEPES, pH 7.2, 750 mM GdnHCl, 2.37 μM Trx-linker pentamer, 2.37 mM Phos-tag-acrylamide, 4.74 mM $ZnCl_2$ ($(Trx\text{-}linker)_5$:Phos-tag-acrylamide:$ZnCl_2$ = 1:1000:2000) (Figure S6). Reducing the cationic electrolyte, $GdnH^+$, and the sulfonate-containing buffering reagent, HEPES, resulted in complete binding (>99% at 2 mM HEPES, pH 7.2, 750 mM KCl, 2.37 μM Trx-linker pentamer, 237 μM Phos-tag-acrylamide, 474 μM $ZnCl_2$ ($(Trx\text{-}linker)_5$:Phos-tag-acrylamide:$ZnCl_2$ = 1:100:200) (Figure S6).

Next, we sought to determine if $PAZn_2$ would enable us to distinguish phosphorylation from a PTM that exhibits a similar ionic blockade.[14] We constructed a Trx-linker pentamer with distinct modification sites in linker 2 (RRASAA) and linker 4 (RRAAAC). We carried out phosphorylation and glutathionylation reactions sequentially to obtain a Trx-linker pentamer with Ser-P in linker 2 and glutathionylated cysteine (Cys-GS) in linker 4 (Figure 2a). In line with the characteristic current patterns recorded separately with Trx-linker nonamers containing a single Ser-P or Cys-GS residue within the same linker sequence,[14] the signals from Ser-P and Cys-GS within the same Trx-linker pentamer exhibited indistinguishable

https://doi.org/10.1021/jacs.4c03912
J. Am. Chem. Soc. 2024, 146, 24265−24270

residual currents and noise when linker 2 and linker 4 were located within the pore (Figure 2a). Pleasingly, the introduction of $PAZn_2$ altered the signal derived from linker 2 to give a pattern similar to that of level A1-P-$PAZn_2$, while the signal from linker 4 was unchanged, allowing clear differentiation between phosphorylation and glutathionylation (Figure 2b).

CONCLUSIONS

Here, we demonstrate the nanopore detection of widely separated phosphorylation sites (e.g., >250 aa apart) within a polypeptide chain by using the Phos-tag dizinc complex (PZn_2) and the Phos-tag-acrylamide dizinc complex ($PAZn_2$). The binder created a distinct two-level current feature when phosphorylated polypeptide segments were inside the nanopore, which resembled current patterns observed during divalent cation chelation within an engineered αHL pore[28] or with amino acids interacting with immobilized Ni^{2+} in an engineered nanopore.[28] We were able to saturate Ser-P with $PAZn_2$ (10 mM HEPES, pH 7.2, 750 mM GdnHCl, 2.37 μM Trx-linker pentamer, 2.37 mM Phos-tag-acrylamide, 4.74 mM $ZnCl_2$ ($(Trx\text{-}linker)_5$:Phos-tag-acrylamide:$ZnCl_2$ = 1:1000:2000). The phosphorylation-specific current feature enabled the discrimination of phosphorylation from PTMs that produced similar current blockades such as glutathionylation. We envision that combinations of PTM-specific binders will allow the simultaneous detection of multiple PTMs. Suitable binders should recognize PTMs irrespective of adjacent amino acid sequences, exhibit fast association and slow dissociation kinetics, and ideally generate characteristic current signatures, such as the subconductance states seen in this work, which facilitate the discrimination of PTMs. Given that most PTMs are enzymatically installed and regulated, they tend to be located within the flexible or exposed regions of proteins.[29] For the small fraction of PTMs that are nonenzymatically installed within the buried regions of proteins (e.g., disulfide bonds), partial unfolding might occur in the presence of chaotropic reagents to allow binder association. So far, we have identified PTMs in polypeptide segments while they are transiently arrested within a nanopore. In our ongoing efforts to study biologically relevant protein targets, the use of bulky binders (e.g., antibodies) holds promise for temporarily halting protein translocation at the pore entrance, thereby mediating PTM identification in any region of a protein.

ASSOCIATED CONTENT

Supporting Information

The Supporting Information is available free of charge at https://pubs.acs.org/doi/10.1021/jacs.4c03912.

Amino acid sequences of the thioredoxin-linker pentamers; and $I_{r.m.s.}$ characteristics of A1-P, A1-P-PZn_2, and A1-P-$PAZn_2$; mean dwell times ($<\tau>$) for two-level A1-P-$PAZn_2$; an SDS-polyacrylamide gel of the Trx-linker pentamer; ESI LC-MS characterization of Trx-linker pentamers; fractions of phosphorylated linkers detected in the $PAZn_2$-bound state in the absence and presence of competing phosphoserine; an ionic current trace showing phosphorylated linkers in excess Zn^{2+} generated similar A1-P current signals; a current trace showing transition between level A1-P-$PAZn_2$ and level A1-P when a phosphorylated segment was inside the $(NN\text{-}113R)_7$ nanopore; fractions of phosphorylated linkers detected in the $PAZn_2$-bound state; and experimental procedures (PDF)

AUTHOR INFORMATION

Corresponding Authors

Hagan Bayley − *Department of Chemistry, University of Oxford, Oxford OX1 3TA, U.K.*; orcid.org/0000-0003-2499-6116; Email: hagan.bayley@chem.ox.ac.uk

Yujia Qing − *Department of Chemistry, University of Oxford, Oxford OX1 3TA, U.K.*; orcid.org/0000-0002-2110-4269; Email: yujia.qing@chem.ox.ac.uk

Authors

Wei-Hsuan Lan − *Department of Chemistry, University of Oxford, Oxford OX1 3TA, U.K.*

Hanxiao He − *Department of Chemistry, University of Oxford, Oxford OX1 3TA, U.K.*

Complete contact information is available at: https://pubs.acs.org/10.1021/jacs.4c03912

Notes

The authors declare the following competing financial interest(s): H.B. is the founder of, a consultant for, and a shareholder of Oxford Nanopore Technologies, a company engaged in the development of nanopore sensing and sequencing technologies. W.-H.L., H.B., and Y.Q., have filed patents describing the binder-assisted PTM detection in electro-osmotically active nanopores and their applications in proteoform characterization.

ACKNOWLEDGMENTS

This research was supported by the Wellcome Leap Delta Tissue Program and Oxford Nanopore Technologies. W.-H.L. is funded by an Oxford-Taiwan Graduate Studentship in partnership with a Department of Chemistry Scholarship, University of Oxford.

REFERENCES

(1) Ramazi, S.; Zahiri, J. Post-translational modifications in proteins: resources, tools and prediction methods. *Database* **2021**, *2021*, No. baab012.

(2) Xu, H.; Wang, Y.; Lin, S.; Deng, W.; Peng, D.; Cui, Q.; Xue, Y. PTMD: a database of human disease-associated post-translational modifications. *Genom. Proteom. Bioinform.* **2018**, *16* (4), 244−251.

(3) Wegmann, S.; Biernat, J.; Mandelkow, E. A current view on Tau protein phosphorylation in Alzheimer's disease. *Curr. Opin. Neurobiol.* **2021**, *69*, 131−138.

(4) Xu, S.; Suttapitugsakul, S.; Tong, M.; Wu, R. Systematic analysis of the impact of phosphorylation and O-GlcNAcylation on protein subcellular localization. *Cell Rep.* **2023**, *42*, No. 112796.

(5) Hu, P.; Shimoji, S.; Hart, G. W. Site-specific interplay between O-GlcNAcylation and phosphorylation in cellular regulation. *FEBS Lett.* **2010**, *584*, 2526−2538.

(6) Nurk, S.; Koren, S.; Rhie, A.; Rautiainen, M.; Bzikadze, A. V.; Mikheenko, A.; Vollger, M. R.; Altemose, N.; Uralsky, L.; Gershman, A.; Aganezov, S.; Hoyt, S. J.; Diekhans, M.; Logsdon, G. A.; Alonge, M.; Antonarakis, S. E.; Borchers, M.; Bouffard, G. G.; Brooks, S. Y.; Caldas, G. V.; Chen, N.-C.; Cheng, H.; Chin, C.-S.; Chow, W.; de Lima, L. G.; Dishuck, P. C.; Durbin, R.; Dvorkina, T.; Fiddes, I. T.; Formenti, G.; Fulton, R. S.; Fungtammasan, A.; Garrison, E.; Grady, P. G. S; Graves-Lindsay, T. A.; Hall, I. M.; Hansen, N. F.; Hartley, G. A.; Haukness, M.; Howe, K.; Hunkapiller, M. W.; Jain, C.; Jain, M.; Jarvis, E. D.; Kerpedjiev, P.; Kirsche, M.; Kolmogorov, M.; Korlach, J.; Kremitzki, M.; Li, H.; Maduro, V. V.; Marschall, T.; McCartney, A. M.; McDaniel, J.; Miller, D. E.; Mullikin, J. C.; Myers, E. W.; Olson,

N. D.; Paten, B.; Peluso, P.; Pevzner, P. A.; Porubsky, D.; Potapova, T.; Rogaev, E. I.; Rosenfeld, J. A.; Salzberg, S. L.; Schneider, V. A.; Sedlazeck, F. J.; Shafin, K.; Shew, C. J.; Shumate, A.; Sims, Y.; Smit, A A. F.; Soto, D. C.; Sovic, I.; Storer, J. M.; Streets, A.; Sullivan, B. A.; Thibaud-Nissen, F.; Torrance, J.; Wagner, J.; Walenz, B. P.; Wenger, A.; Wood, J. M. D; Xiao, C.; Yan, S. M.; Young, A. C.; Zarate, S.; Surti, U.; McCoy, R. C.; Dennis, M. Y.; Alexandrov, I. A.; Gerton, J. L.; O'Neill, R. J.; Timp, W.; Zook, J. M.; Schatz, M. C.; Eichler, E. E.; Miga, K. H.; Phillippy, A. M. The complete sequence of a human genome. *Science* **2022**, *376* (6588), 44−53.

(7) Parker, M. T.; Knop, K.; Sherwood, A. V.; Schurch, N. J.; Mackinnon, K.; Gould, P. D.; Hall, A. J. W.; Barton, G. J.; Simpson, G. G. Nanopore direct RNA sequencing maps the complexity of Arabidopsis mRNA processing and m^6A modification. *Elife* **2020**, *9*, No. e49658.

(8) Rodriguez-Larrea, D.; Bayley, H. Multistep protein unfolding during nanopore translocation. *Nat. Nanotechnol.* **2013**, *8* (4), 288−295.

(9) Rosen, C. B.; Rodriguez-Larrea, D.; Bayley, H. Single-molecule site-specific detection of protein phosphorylation with a nanopore. *Nat. Biotechnol.* **2014**, *32* (2), 179−181.

(10) Ying, Y. L.; Hu, Z. L.; Zhang, S.; Qing, Y.; Fragasso, A.; Maglia, G.; Meller, A.; Bayley, H.; Dekker, C.; Long, Y. T. Nanopore-based technologies beyond DNA sequencing. *Nat. Nanotechnol.* **2022**, *17* (11), 1136−1146.

(11) Restrepo-Pérez, L.; Joo, C.; Dekker, C. Paving the way to single-molecule protein sequencing. *Nat. Nanotechnol.* **2018**, *13* (9), 786−796.

(12) Nivala, J.; Marks, D. B.; Akeson, M. Unfoldase-mediated protein translocation through an α-hemolysin nanopore. *Nat. Biotechnol.* **2013**, *31* (3), 247−250.

(13) Yu, L.; Kang, X.; Li, F.; Mehrafrooz, B.; Makhamreh, A.; Fallahi, A.; Foster, J. C.; Aksimentiev, A.; Chen, M.; Wanunu, M. Unidirectional single-file transport of full-length proteins through a nanopore. *Nat. Biotechnol.* **2023**, *41* (8), 1130−1139.

(14) Martin-Baniandres, P.; Lan, W.-H.; Board, S.; Romero-Ruiz, M.; Garcia-Manyes, S.; Qing, Y.; Bayley, H. Enzyme-less nanopore detection of post-translational modifications within long polypeptides. *Nat. Nanotechnol.* **2023**, *18*, 1335−1340.

(15) Sauciuc, A.; Morozzo della Rocca, B.; Tadema, M. J.; Chinappi, M.; Maglia, G. Translocation of linearized full-length proteins through an engineered nanopore under opposing electrophoretic force. *Nat. Biotechnol.* **2023**, DOI: 10.1038/s41587-023-01954-x.

(16) Restrepo-Pérez, L.; Wong, C. H.; Maglia, G.; Dekker, C.; Joo, C. Label-free detection of post-translational modifications with a nanopore. *Nano Lett.* **2019**, *19* (11), 7957−7964.

(17) Ensslen, T.; Sarthak, K.; Aksimentiev, A.; Behrends, J. C. Resolving isomeric posttranslational modifications using a biological nanopore as a sensor of molecular shape. *J. Am. Chem. Soc.* **2022**, *144* (35), 16060−16068.

(18) Nova, I. C.; Ritmejeris, J.; Brinkerhoff, H.; Koenig, T. J. R.; Gundlach, J. H.; Dekker, C. Detection of phosphorylation post-translational modifications along single peptides with nanopores. *Nat. Biotechnol.* **2024**, *42*, 710−714.

(19) Cao, C.; Magalhães, P.; Krapp, L. F.; Bada Juarez, J. F.; Mayer, S. F.; Rukes, V.; Chiki, A.; Lashuel, H. A.; Dal Peraro, M. Deep learning-assisted single-molecule detection of protein post-translational modifications with a biological nanopore. *ACS Nano* **2024**, *18* (2), 1504−1515.

(20) Kinoshita, E.; Takahashi, M.; Takeda, H.; Shiro, M.; Koike, T. Recognition of phosphate monoester dianion by an alkoxide-bridged dinuclear zinc(II) complex. *Dalton Trans.* **2004**, *8*, 1189−1193.

(21) Takiyama, K.; Kinoshita, E.; Kinoshita-Kikuta, E.; Fujioka, Y.; Kubo, Y.; Koike, T. A phos-tag-based fluorescence resonance energy transfer system for the analysis of the dephosphorylation of phosphopeptides. *Anal. Biochem.* **2009**, *388*, 235−241.

(22) Gu, L.-Q.; Cheley, S.; Bayley, H. Electroosmotic enhancement of the binding of a neutral molecule to a transmembrane pore. *Proc. Natl. Acad. Sci. U. S. A.* **2003**, *100* (26), 15498−15503.

(23) Kinoshita, E.; Kinoshita-Kikuta, E.; Koike, T. Separation and detection of large phosphoproteins using Phos-tag SDS-PAGE. *Nat. Protoc.* **2009**, *4* (10), 1513−1521.

(24) Kinoshita-Kikuta, E.; Kinoshita, E.; Koike, T. Neutral phosphate-affinity SDS-PAGE system for profiling of protein phosphorylation. *Methods Mol. Biol.* **2015**, *1295*, 323−354.

(25) Takeda, H.; Kawasaki, A.; Takahashi, M.; Yamada, A.; Koike, T. Matrix-assisted laser desorption/ionization time-of-flight mass spectrometry of phosphorylated compounds using a novel phosphate capture molecule. *Rapid Commun. Mass Spectrom.* **2003**, *17* (18), 2075−2081.

(26) Hammerstein, A. F.; Shin, S. H.; Bayley, H. Single-molecule kinetics of two-step divalent cation chelation. *Angew. Chem., Int. Ed.* **2010**, *49*, 5085−5090.

(27) Ojida, A.; Mito-Oka, Y.; Sada, K.; Hamachi, I. Molecular recognition and fluorescence sensing of monophosphorylated peptides in aqueous solution by bis(zinc(II)-dipicolylamine)-based artificial receptors. *J. Am. Chem. Soc.* **2004**, *126* (8), 2454−2463.

(28) Wang, K.; Zhang, S.; Zhou, X.; Yang, X.; Li, X.; Wang, Y.; Fan, P.; Xiao, Y.; Sun, W.; Zhang, P.; Li, W.; Huang, S. Unambiguous discrimination of all 20 proteinogenic amino acids and their modifications by nanopore. *Nat. Methods* **2024**, *21*, 92−101.

(29) Hornbeck, P. V.; Zhang, B.; Murray, B.; Kornhauser, J. M.; Latham, V.; Skrzypek, E. PhosphoSitePlus, 2014: mutations, PTMs and recalibrations. *Nucleic Acids Res.* **2015**, *43* (Database issue), D512−D520.

https://doi.org/10.1021/jacs.4c03912
J. Am. Chem. Soc. 2024, 146, 24265−24270